Solid−Fluid and Solid−Solid Equilibrium in Hard Sphere United Atom Models of *n*-Alkanes: Rotator Phase Stability[†]

M. Cao and P. A. Monson*

Department of Chemical Engineering, University of Massachusetts, Amherst, Massachusetts 01003

Received: March 31, 2009; Revised Manuscript Received: June 1, 2009

We present a study of the phase behavior for models of *n*-alkanes with chain lengths up to C_{21} based on hard sphere united atom models of methyl and methylene groups, with fixed bond lengths and C−C−C bond angles. We extend earlier work on such models of shorter alkanes by allowing for gauche conformations in the chains. We focus particularly on the orientational order about the chain axes in the solid phase near the melting point, and our model shows how the loss of this orientational order leads to the formation of rotator phases. We have made extensive calculations of the thermodynamic properties of the models as well as order parameters for tracking the degree of orientational order around the chain axis. Depending on the chain length and whether the carbon number is even or odd, the model exhibits both a rotator phase and a more orientationally ordered solid phase in addition to the fluid phase. Our results indicate that the transition between the two solid phases is first-order with a small density change. The results are qualitatively similar to those seen experimentally and show that rotator phases can appear in models of alkanes without explicit treatment of attractive forces or explicit treatment of the hydrogen atoms in the chains.

I. Introduction

The solid phases of *n*-alkanes continue to be of interest for a number of reasons. They are important components of petroleum solids such as waxes. They are model compounds for understanding the properties of polymers. The lamellar structures that appear as *n*-alkane solids are model structures for understanding lamellar structures in other systems, such a lipoprotein membranes. Finally, the solid−fluid and solid−solid phase behavior show clear and systematic changes with chain length, and it is important to investigate whether such behavior can be captured by molecular models. The shorter-chain *n*-alkanes have odd−even trends on their melting or triple points,[1,2] and rotator phases appear for longer *n*-alkanes between the isotropic fluid phase and the fully ordered solid phase (which we will refer to as the crystalline solid).[3−19] The rotator phases are characterized by the chains' losing the orientational order around their chain axes while maintaining their translational order. Five types of rotator phases have been reported in the literature, differing from each other by different tilt angles relative to the lamellar planes in the solid and also by different layer packing. Properties of rotator phases have been determined in a number of molecular simulation studies[20−27] which showed that structural properties of these phase can be captured by molecular models of *n*-alkane chains. However, these studies did not feature phase equilibrium calculations to investigate thermodynamic stability.

We have previously used Monte Carlo simulations to study the solid−fluid equilibrium for models of *n*-alkanes with chain lengths up to C_8, including some studies of mixtures.[1,28−30] Our models used united atom models of the methyl and methylene groups, with hard sphere packing and with fixed bond lengths and C−C−C bond angles. To model the chain flexibility, three types of torsional potentials were considered. This relatively simple approach, which is based on the idea that the structure of condensed phases should be dominated by molecular packing associated with short-range repulsive interactions, was found to be capable of describing the odd−even trends in the solid−fluid equilibrium. These trends were related to how the solid phase structure was determined by the chain packing for the odd and even chain lengths. In the present work, we extend this approach to longer chains and, in particular, to the stability of rotator phases.

We have considered chain lengths between C_9 and C_{21}. To describe the chain flexibility, we use a modification of model II from ref 1. In this model, a hard core interaction between pairs of sites separated by two other sites within a chain determines the torsional potential. This leads to chains that can adopt conformations corresponding to small fluctuations about the all-trans conformation. For the shorter chains considered in our earlier work, the appearance of gauche conformations is of relatively low probability, and this assumption is qualitatively reasonable. For longer chains, especially in the fluid phase, this is no longer the case, and we have developed a torsional potential for this case that allows for gauche conformations while staying within the spirit of model II of ref 1.

We have found that our hard sphere chain models of *n*-alkanes can, indeed, capture the stability of a rotator phase for longer chain lengths. This stability is especially favored in the odd-chain-length systems in which the chain axes tend to lie perpendicular to the plane of the lamellae in the solid structure. However, we also find a rotator phase for longer chain lengths with an even carbon number. For these systems, a monoclinic solid structure starts to be more stable than the triclinic structure, which is stable for shorter chain lengths. In this latter structure, the chain axes are tilted away from the normal to the lamellar planes. The domains of stability of the rotator phase for the odd and even chain lengths of our model, while not precisely the same as those seen experimentally for the *n*-alkanes, are qualitatively quite similar, and the model seems to give a good description of the underlying physics. The rotator phase we have

[†] Part of the "H. Ted Davis Special Section".

* To whom correspondence should be addressed. E-mail: monson@ecs.umass.edu.

10.1021/jp902887w CCC: $40.75
Published on Web 07/17/2009

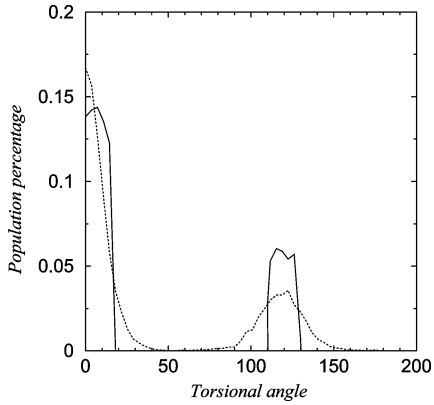

Figure 1. Schematic diagram of population of molecules in trans and gauche configurations for a C_{20} system. Dashed line: model III at $P\sigma^3/kT = 4$, $T = 300$ K. Solid line: model IV at $P\sigma^3/kT = 4$.

found for odd carbon numbers is similar to the R I phase identified in experiments[3−19] but differs due to its triclinic versus orthorhombic symmetry (we have not found an equivalent of the R II phase).[10] The rotator phase found for even carbon numbers is a monoclinic structure, which might be related to the monoclinic R IV phase identified for C_{28} and C_{30} systems.[11]

Our paper is organized as follows: In section II, we describe the molecular model, the solid structures we have found for the model, and how they relate to the structures of real alkanes. In section II, we also describe the simulation methodologies and their implementation for this model. The results are presented in section III, and section IV gives a summary of our results and our conclusions.

II. Models and Methods

A. Molecular Models. The *n*-alkane model used here follows that used in earlier work.[1] Methyl and methylene groups are represented by hard spheres of diameter σ separated by a distance $l = 0.4\sigma$. The C−C−C bond angles are fixed at the value for tetrahedral coordination. The treatment of chain flexibility is based on model II of ref 1, in which we use a hard sphere interaction with collision diameter σ between sites separated by two or more sites. As mentioned earlier, this model allows for small departures from the all-trans conformation, but gauche conformations are excluded. To include gauche conformations, we could include a torsional potential, such as those used in more realistic models,[31,32] as was done in model III of ref 1. In this work, we use an alternative approach that keeps us in the spirit of model II and maintains the athermal nature of the flexibility. We define the torsional potential as

$$U(\phi) = \begin{cases} 0 & \text{if } |\phi| < \phi_1 \text{ or } |\phi - 120°| < \phi_2 \\ \infty & \text{otherwise} \end{cases}$$

where ϕ is the torsional angle. We chose $\phi_1 = 17.4$, which is based on the torsional angle restrictions emerging in model II of ref 1 and $\phi_2 = 10$ to give an appropriate ratio of population for the trans and gauche states. Figure 1 shows the torsional angle distribution for this model as compared with that of model III of ref 1 for a C_{20} system at the state of $P\sigma^3/kT = 4$, $T = 300$ K. The Padilla−Toxvaerd[32] torsional potential was used in model III. The new model gives a good estimate of the relative populations of the trans and gauche states as compared with model III. For consistency with the earlier work, we will refer to this new model as model IV.

B. Solid Phase Free energy Calculation. The free energy was calculated at each phase to determine the phase equilibrium properties. Thermodynamic integration methods were used. In the fluid phase, the reference state is the ideal gas. For solid phases, the reference free energy was calculated through the method proposed by Frenkel and Ladd,[34] as adapted to these kinds of models of *n*-alkanes by Malanoski and Monson.[1] We refer the reader to ref 1 for complete details. The interacting Einstein crystal Hamiltonian is given by

$$H_{i,e} = H_0 + \sum_{i=1}^{N} \left[\lambda(\mathbf{r}_i - \mathbf{r}_i^0)^2 + \sum_{j=2}^{n} \lambda(\mathbf{r}_{ij} - \mathbf{r}_{ij}^0)^2 \right] \tag{1}$$

where H_0 is the Hamiltonian for the hard chain system, $\mathbf{r}_i$ gives the position of one reference site in the ith chain, and $\mathbf{r}_i^0$ is the position of this site in the static lattice. $\mathbf{r}_{ij}$ is the vector pointing from the reference site in the ith chain to the jth site in the same chain, and $\mathbf{r}_{ij}^0$ is the reference vector. In all cases, including the rotator phases, we used a fully ordered crystal structure to give the reference coordinates. The free energy difference between the Einstein crystal and the solid of interest is calculated in a series of steps. The first step is to compute the free energy difference between the solid of interest and the solid with a fixed center of mass. This contribution is given by[35]

$$\frac{\Delta A_1}{NkT} = -\frac{\ln V/N}{N} \tag{2}$$

where V is the volume of the system and N is the total number of molecules. The second step is to calculate the free energy difference between the solid with fixed center of mass and an interacting Einstein crystal with fixed center of mass, and this free energy difference can be written as

$$\frac{\Delta A_2}{NkT} = -\frac{1}{N}\int_0^{\lambda_{\max}} \left\langle \sum_{i=1}^{N} \left[(\mathbf{r}_i - \mathbf{r}_i^0)^2 + \sum_{j=2}^{n} (\mathbf{r}_{ij} - \mathbf{r}_{ij}^0)^2 \right] \right\rangle_\lambda \mathrm{d}\lambda \tag{3}$$

Here, $\lambda_{\max}$ is a value of λ sufficiently large that the system properties are very close to those of the Einstein crystal. The angle brackets denote the (N, V, T) ensemble average. The integration can be calculated numerically with a series of ensemble averages obtained from Monte Carlo simulations at different λ. The third step is the free energy difference between the interacting Einstein crystal and the ideal Einstein crystal. This term can be written as

$$\frac{\Delta A_3}{NkT} = -\frac{1}{N}\ln\langle e^{-\beta H_0}\rangle_{n.e} \tag{4}$$

n.e denotes the average is taken in the system without intermolecular interactions. When the λ is large enough, this contribution becomes very small. The next contribution is from the free energy change when the body fixed component of the Einstein crystal external fields are switched off. In Malanoski and Monson's work, this contribution was obtained via[1]

$$\frac{\Delta A_4}{NkT} = \ln\left[\frac{\int d\mathbf{r}_{12} \ldots d\mathbf{r}_{1n} \exp(-\beta U_{\text{intra}}) \exp\left[-\lambda_{\max} \sum_{j=2}^{n} (\mathbf{r}_{1j} - \mathbf{r}_{1j}^0)^2\right]}{\int d\mathbf{r}_{12} \ldots d\mathbf{r}_{1n} \exp(-\beta U_{\text{intra}})}\right] \quad (5)$$

Both the denominator and numerator can be calculated individually by Monte Carlo integration over states of single chains. However, this method becomes inefficient when the intramolecular potential permits gauche conformers, especially for longer chains, due to the much larger regions of configuration space that are now accessible to the chain relative to the regions of configuration space where the integrand in the numerator has significant values. To obtain more accurate results, another approach is needed. The idea is that instead of calculating ΔA_4 for model IV, we calculate it for model II. Then the difference between those two terms can be obtained from the difference between the isolated single chain free energies of models IV and II. To distinguish the ΔA_4 term in different models, we use superscripts IV and II. In this way, ΔA_4^{IV} can be expressed as

$$\Delta A_4^{\text{IV}} = A_{\text{sc}}^{\text{IV}}(\lambda_{\max}) - A_{\text{sc}}^{\text{IV}}(0) = [A_{\text{sc}}^{\text{IV}}(\lambda_{\max}) - A_{\text{sc}}^{\text{II}}(\lambda_{\max})] + [A_{\text{sc}}^{\text{II}}(\lambda_{\max}) - A_{\text{sc}}^{\text{II}}(0)] + [A_{\text{sc}}^{\text{II}}(0) - A_{\text{sc}}^{\text{IV}}(0)] = [A_{\text{sc}}^{\text{IV}}(\lambda_{\max}) - A_{\text{sc}}^{\text{II}}(\lambda_{\max})] + \Delta A_4^{\text{II}} + [A_{\text{sc}}^{\text{II}}(0) - A_{\text{sc}}^{\text{IV}}(0)] \quad (6)$$

where $A_{\text{sc}}^{\text{IV}}$ and $A_{\text{sc}}^{\text{II}}$ are the single chain free energies for models IV and II, respectively. and the superscripts IV and II are used to indicate models IV and model II, respectively. The numbers in parentheses give the strengths of the Einstein field. For instance, $A_{\text{sc}}^{\text{IV}}(\lambda)$ indicates the free energy of single chain with model IV in the Einstein field with coupling constant λ. The term $A_{\text{sc}}^{\text{IV}}(\lambda_{\max}) - A_{\text{sc}}^{\text{II}}(\lambda_{\max})$ in eq 6 can be neglected for sufficiently large $\lambda_{\max}$, since the Einstein field strongly favors the all-trans chain conformations. ΔA_4^{II} can be computed using eq 5. However, we have found that for longer-chain systems, the precision of the results can be improved by using a coupling parameter integration via

$$\frac{\Delta A_4^{\text{II}}}{NkT} = \int_0^{\lambda_{\max}} \left\langle \sum_{j=2}^{n} (\mathbf{r}_{ij} - \mathbf{r}_{ij}^0)^2 \right\rangle_\lambda d\lambda \quad (7)$$

The term in angled brackets is obtained from Monte Carlo simulations at various values for λ from 0 to $\lambda_{\max}$ for the single chain, and the free energy difference is calculated using numerical integration. The last term in eq 6, $A_{\text{sc}}^{\text{II}}(0) - A_{\text{sc}}^{\text{IV}}(0)$, can be obtained from individual calculations for $A_{\text{sc}}^{\text{II}}(0)$ and $A_{\text{sc}}^{\text{II}}(0)$ using Monte Carlo integration. The final contribution is the free energy of an ideal Einstein crystal of N atoms with a fixed center of mass, A_{E}. Expressions for this are given by Frenkel and coworkers.[35] We then have

$$A = \Delta A_1 + \Delta A_2 + \Delta A_3 + \Delta A_4 + A_{\text{E}} \quad (8)$$

C. Order Parameter Calculation. To monitor orientational order around the chain axes, we used an order parameter defined as

$$S = \left(\frac{\sum_i^N \sin\theta_i}{N}\right)^2 + \left(\frac{\sum_i^N \cos\theta_i}{N}\right)^2 \quad (9)$$

where θ_i is the angle between the orientation of the chain i with the orientation of that chain in the reference lattice. This angle is defined using the first two bond vectors of each chain via

$$\cos\theta = \frac{1}{l^4}(\mathbf{r}_{1,2} \times \mathbf{r}_{2,3}) \cdot (\mathbf{r}_{1,2}^0 \times \mathbf{r}_{2,3}^0) \quad (10)$$

where, for example, $\mathbf{r}_{1,2} = \mathbf{r}_2 - \mathbf{r}_1$ is the vector between the first two sites in the chain and the 0 superscript denotes that vector for the fully ordered solid. We have $S = 1$ if the system is fully orientationally ordered, and $S = 0$, when the system has orientational disorder around the chain axes. For chains with an odd carbon number, we modify the definition to take into account the different chain axis orientations in alternate layers of the solid. We then have

$$S = \frac{1}{m}\sum_j^m \left[\left(\frac{\sum_i^{N_m} \sin\theta_i}{N_m}\right)^2 + \left(\frac{\sum_i^{N_m} \cos\theta_i}{N_m}\right)^2\right] \quad (11)$$

where m denotes the total number of chain orientations in the perfectly ordered crystal, and $N_m = N/m$ is the number of chains in each of these orientations.

D. Monte Carlo Simulation Details. Monte Carlo simulations in the isobaric, isothermal (NPT) ensemble were employed to calculate the pressure−density isotherms of the models for different chain lengths. Simulations were carried out for both solid and fluid phases: 432 molecules were used for even-carbon-number, solid phase simulations, and 384 molecules were used for odd-carbon-number, solid-phase simulations. For the fluid phase, normally, 512 chains were studied. Typically 400 000 cycles were performed to equilibrate the system and another 400 000 cycles for obtaining averages. A cycle involves N attempts to move chains and one attempt to change the volume of the system (N is the total number of the chains in the system). Trial moves included single-chain translation, single-chain rotation around the center of mass, configurational bias moves,[36] and chain rotation around the chain axes. The probabilities to attempt these moves were the same. We have found that simulations without chain rotations needed more configurations to equilibrate. The maximum displacements were chosen so that the acceptance ratios for translation and rotation moves were all about 20% and 10% for the volume changes. Volume shifts in the fluid phase were isotropic. For solid phases, anisotropic volume changes developed by Parrinello and Rahman[39] were included to sample fluctuations in the solid phase geometry. The simulations in the fluid phases started from low density states, and the systems were progressively compressed to higher density. We also expanded the systems from higher pressure states and obtained densities similar to those obtained during the compression procedure, indicating that the dense fluid states lie on a reversible path. The solid phase equations of state were obtained from an expansion initially starting from close packed structures. The initial configuration of each simulation point was taken from the final configuration of a previous simulation. More points were simulated in the low pressure region to capture the subtle density changes around the melting point and rotator

TABLE 1: Coefficients for the Rational Function Fits of the Equations of the State for Fluid Phase from MC Simulation

	C_0	C_1	C_2	C_3	C_4
C_{13}	6.827 224 15	31.520 333 2	−77.171 345 7	101.505 258	1.197 129 34
C_{15}	11.695 846 7	63.911 250 7	−167.761 113	268.407 330	1.362 039 68
C_{17}	2.471 519 52	10.865 544 7	−29.012 499 6	14.548 405 2	0.879 140 393
C_{18}	1.713 457 39	6.998 577 63	−28.193 385 1	19.750 764 9	0.781 824 904
C_{19}	4.926 559 61	0.374 916 904	−3.200 099 99	−4.388 067 31	0.912 362 108
C_{20}	2.361 253 43	10.673 612 5	−32.874 099 7	18.797 962 2	0.838 031 940
C_{21}	5.594 355 70	−0.220 119 576	−0.737 116 481	−7.288 420 79	0.916 338 874

TABLE 2: Coefficients for the Rational Function Fits of the Equations of the State for Rotator Phase from MC Simulation

	C_0	C_1	C_2	C_3	C_4
C_{13}	2.56122723	−3.41541914	−4.54072117	6.01258602	0.750711164
C_{15}	2.54472401	−3.03516561	−4.04720977	4.64392807	0.772277064
C_{17}	2.03901472	−2.64025867	−2.96955921	3.71273402	0.754738836
C_{19}	1583.17277	−7245.98603	11082.0529	−5653.89028	0.975016811
C_{20}	173.084449	−271.597453	−309.499044	521.215235	1.12631328
C_{21}	−63.7815671	120.124132	130.693204	−230.313201	1.06973491

TABLE 3: Coefficients for the Rational Function Fits of the Equations of the State for Ordered Crystal Phase from MC Simulation

	C_0	C_1	C_2	C_3	C_4
C_{13}	3.598 058 97	−4.072 638 89	−5.087 467 56	5.734 617 00	0.837 025 044
C_{15}	150.741 470	−557.954 017	690.132 627	−282.102 381	0.959 620 716
C_{17}	3.873 550 46	−4.268 913 39	−5.818 322 75	6.414 615 97	0.836 530 776
C_{18}	184.610 392	−697.263 864	882.433 231	−370.908 888	0.969 286 959
C_{19}	185.678 857	−702.641 598	890.812 011	−375.927 556	0.941 933 957
C_{20}	4.051 848 50	−4.800 787 70	−5.871 511 42	6.944 785 50	0.827 191 789
C_{21}	55.770 942 2	−205.980 584	260.192 623	−111.180 746	0.910 827 875

phase states. Some compression simulations were also performed in the solid phase.

Equation of state data in each phase were fitted with rational function expressions for convenience in calculating the phase coexistence. The fits give the compressibility factor, Z, as functions of the volume fraction, y. For the fluid phase data, we used

$$Z = \frac{c_0{}^3 + c_1 y + c_2 y^2 + c_3 y^3 + c_4 y^4}{(c_0 - y)^3} \qquad (12)$$

and we used

$$Z = \frac{c_1 y + c_2 y^2 + c_3 y^3 + c_4 y^4}{(c_0 - y)^3} \qquad (13)$$

for the solid phase data. Tables 1−3 contain values of coefficients for eqs 12 and 13 for *n*-alkanes of different chain lengths.

After calculating the free energy for one particular density, thermodynamic integration was used to calculate the solid free energy at other densities. In some cases, free energies were calculated directly at more than one density to check for the thermodynamic consistency. Values for the reference free energies are given in Table 4. From the free energy and equation of state, we calculated the chemical potentials.

As described earlier, the solid free energy was calculated using the thermodynamic integration methodology by Frenkel and Ladd.[34] Even with the modifications described above, efficient sampling is difficult for longer chains. For instance, the mean square displacement of the chains at strong Einstein field approaches its equilibrium value very slowly, and the acceptance ratio for configurational bias is extremely small. To overcome those problems, we decided to use much longer simulation runs but for smaller system sizes: 75 molecules for even carbon numbers and 64 molecules for odd numbers. To improve the efficiency of configurational-bias moves, the Einstein field was applied during the Rosenbluth factor calculations. Typically, 10^6 cycles were used to equilibrate the system, and another 10^6 cycles were used to obtain the ensemble average. More cycles were used in the simulation when λ was very large and configurational bias was not efficient.

TABLE 4: Helmholtz Free Energies for Solids Calculated from MC Techniques[a]

solid	N	λ	$\rho\sigma^3$	A_E	ΔA_2	ΔA_4	A_{ref}
C_{17} (c)	64	35 000	0.1395	13.856	65.04	−54.6	29.7
C_{17} (r)	64	35 000	0.1271	13.856	65.04	−48.5	23.6
C_{18} (c)	75	35 000	0.1367	13.877	67.04	−47.3	33.1
C_{19} (c)	64	35 000	0.1268	13.856	69.13	−58.0	32.8
C_{19} (r)	64	35 000	0.1113	13.856	69.13	−49.5	24.0
C_{20} (c)	75	35 000	0.1253	13.877	71.30	−60.1	37.8
C_{20} (r)	75	35 000	0.1059	13.877	71.30	−46.7	24.4
C_{21} (c)	64	35 000	0.1199	13.856	73.43	−61.3	40.1
C_{21} (r)	64	35 000	0.1006	13.856	73.43	−46.5	24.3

[a] The letters in parentheses indicate whether the solid phase was a "crystal" or "rotator" phase. The estimated uncertainty in the numbers in the final column is in the neighborhood of 1%.

III. Results

A. Solid Phase Structures. The use of hard sphere chain models for *n*-alkane solids is closely related to the maximum close packing principle proposed by Kitaigorodsky.[33] It is anticipated that the structure that allows the chains to achieve their highest density in the limit of very high pressure will be the most stable structure, since it will likely lead to the highest amount of accessible configuration space at lower pressures. The stability of cubic close packing of hard spheres follows

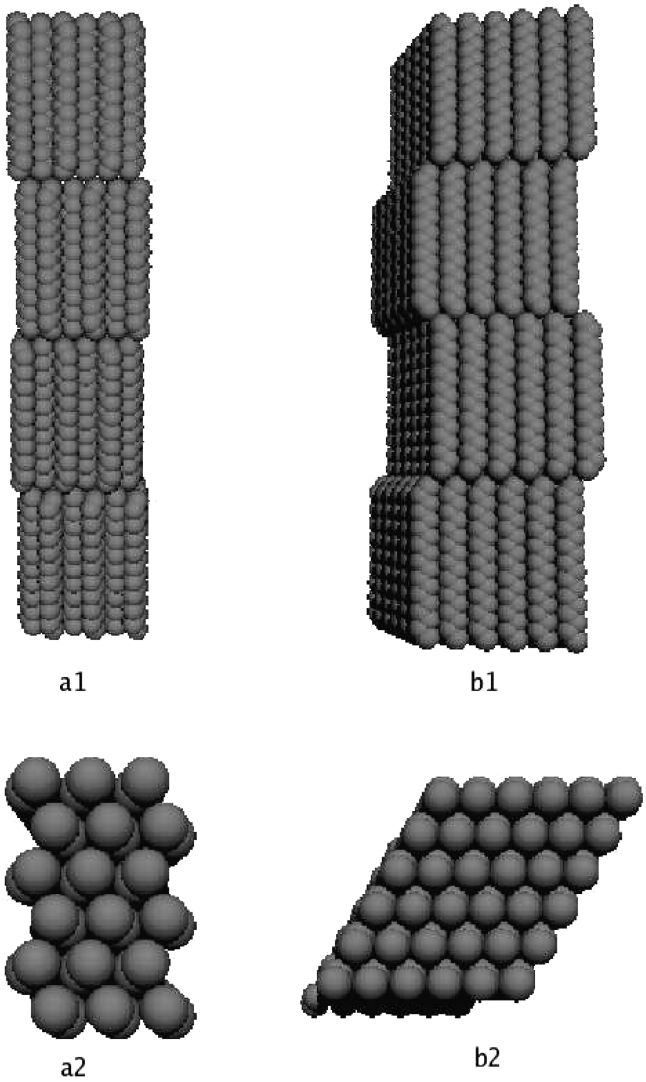

Figure 2. Solid structures for odd-carbon-number *n*-alkanes. a1 and a2 show the hard core model C_{19} in the orthorhombic crystal structure. a1 shows the chain layer stacking, a2 shows the cross section perpendicular to chain axes. b1 and b2 show the hard core model C_{19} in the triclinic crystal structure. b1 shows the layer and b2 shows the cross section perpendicular to the chain axes.

from this. We have used a previously developed simulated annealing method[1] to search for close packed structures, with experimental structures used for starting points. The space group symmetries were maintained during the annealing process. Experimental studies show that odd-carbon-number alkanes for $n-C_9H_{20}$ and beyond have orthorhombic crystal structures, with a space group of *Pbcm*.[5] All the molecules are packed into layers with their chain axes perpendicular to the layer interface. Within each layer, the molecules form a herringbone pattern.[5,24] The structure is illustrated in Figure 2 using the hard core chain model. The solid structures of odd-carbon-number *n*-alkanes derived from our work are somewhat different from the experimentally determined ones. In the experimental structures, the molecules pack into A−B−A−B layers, and in each layer, molecules organize themselves into two different orientations. Our model also gives rise to molecules packed into A−B−A−B layers but in a triclinic structure with space group $P\bar{1}$, which is the space group for shorter odd carbon number *n*-alkanes[2] and shown in Figure 2.

For even-carbon-number *n*-alkanes, two crystal structures, triclinic and monoclinic, have been reported experimentally, and

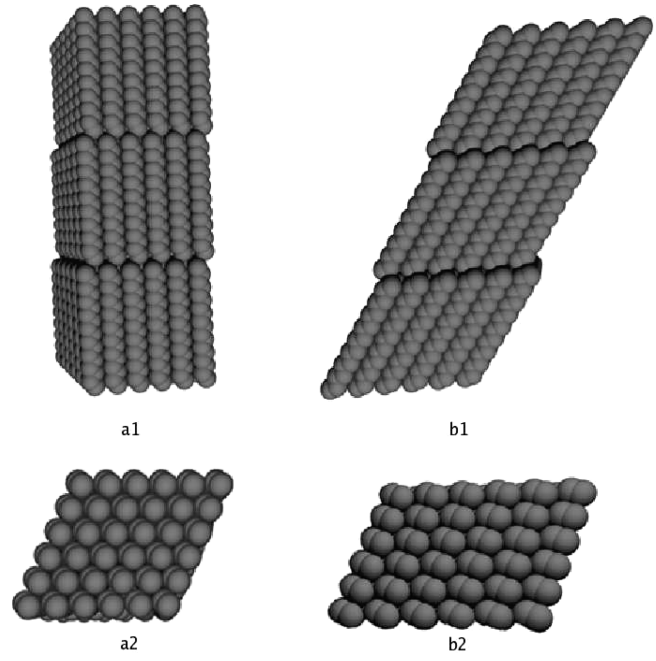

Figure 3. Solid structures for even-carbon-number *n*-alkanes. a1 and a2 show the hard core model C_{18} in the monoclinic crystal structure. a1 shows the layer structure, and a2 shows the cross section. b1 and b2 show hard core model C_{18} in triclinic structure. b1 shows the layer structure, and b2 shows the cross section.

those are shown in Figure 3. The triclinic structure has been observed for the chain lengths below C_{24}, and the monoclinic structure is stable above chain length of C_{26}. Both structures have been seen for C_{24} and C_{26} in experiments.[33,37,38] For even-carbon-number chains, our model also exhibits either a triclinic solid or a monoclinic solid. We have found that the triclinic structure has a slightly higher close packed density than the monoclinic structure when the carbon number is less than 20. For carbon numbers ≥ 20, the close packed densities for the two structures are very similar.

B. Phase Behavior. ***1. Odd Carbon Numbers.*** We used NPT Monte Carlo simulations to obtain the pressure−density equation of state for the solid and fluid phases. The equation of state obtained from the simulation has a shape similar to those found earlier for shorter chains.[1] However, the pressure density isotherm for the solid is not smooth: there seems to be a small transition at low-density solid, as illustrated in Figure 4 for the C_{17} system. When we compressed the low-density solid, there was a small hysteresis in a narrow range of pressures. The order parameter versus pressure diagram for the same system is shown in Figure 5, showing the loss of orientational order as the pressure is reduced. To give a better illustration, we show two snapshots taken from simulation in Figure 4. One is from the high pressure, where the orientational order still persists; the other one is from a lower pressure, where the molecules lose orientational order around the chain axis.

The chemical potentials for C_{17} vs pressure are shown in Figure 6. There are three lines in the figure, corresponding to the free energy of fluid, crystalline solid, and rotator phase. The equation of state as well as the crystal−rotator phase and rotator−fluid phase transitions for C_{17} are shown in Figure 7. The density change due to the phase transition between the rotator phase and crystalline phase is much smaller than the density change for the phase transition of the rotator phase to the fluid phase. Notice that the pressure associated with the solid−solid phase transition is consistent with the pressure range

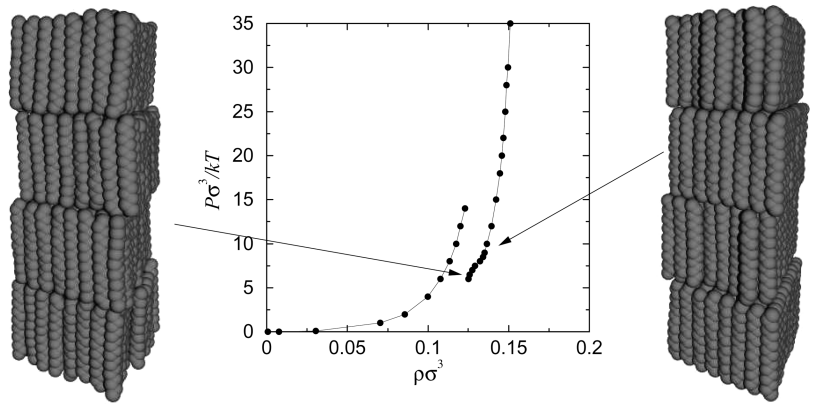

Figure 4. Solid structures for the C_{17} model at different pressures in relation to the pressure−density equation of state.

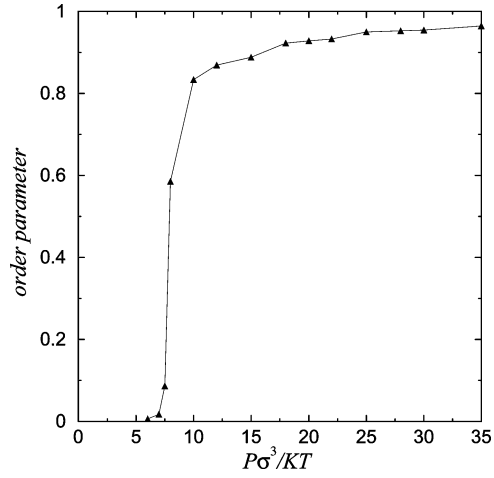

Figure 5. Order parameter versus density for the C_{17} model in the solid phase. Notice that the loss of orientational order correlates with the density change in Figure 4.

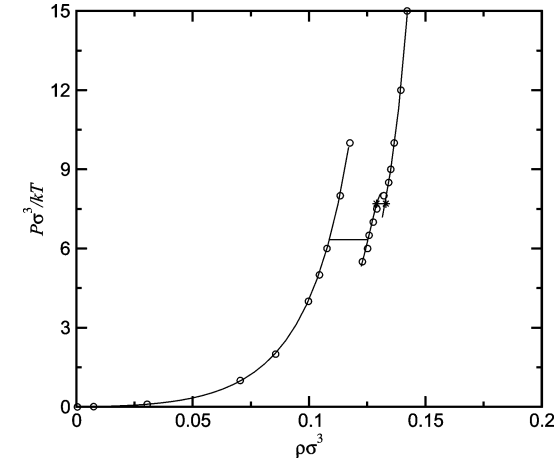

Figure 7. Pressure−density equation of state of the C_{17} system. The points are our Monte Carlo simulation results, and the lines give the fits from eqs 12 and 13. The phase transitions are indicated by horizontal lines. the uncertainty in the density is much smaller than the symbol size used in the figure.

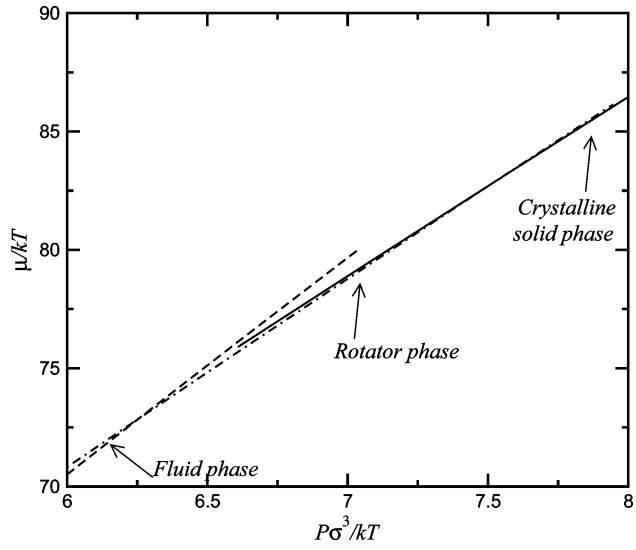

Figure 6. Chemical potential versus pressure for the C_{17} model in each phase. Dashed line, fluid phase; long dashed line, rotator phase; solid line, crystalline phase. Phase transitions are marked by the crossing of these lines.

where the orientational order parameter shows a transition from high to low values, as shown in Figure 5. The primary source of uncertainty in the location of the phase transition comes from the uncertainty in the Helmholtz energy of the solid phases. This leads to an uncertainty of about $\pm 0.3kT$ in the chemical potentials of those phases, which translates to an uncertainty of about $\pm 0.1kT/\sigma^3$ in the transition pressure.

Having established the stability of a rotator phase for the model, we set out to identify the chain length at which the rotator phase becomes stable. We show the phase diagram of C_{13} in Figure 8. This figure shows that the *n*-alkane of this chain length melts to the fluid directly without passing through a stable rotator phase. The rotator phase can be seen in our simulations, as is evident from the solid branch of the equation of state at lower pressures, but it is metastable. We present the phase diagram of C_{15} in Figure 9. It reproduces the phenomena we have seen for C_{17} with a thermodynamically stable rotator phase.

Thus, we see that for odd carbon numbers, our model predicts the stability of a rotator phase for chain lengths greater than or equal to C_{15}. This is a higher chain length than that seen experimentally where the rotator phase is stable for C_9 and higher.[8] However, we have found that the rotator phase is at least metastable for all chain lengths studied.

2. Even Carbon Numbers. Here, we focus on C_{18} and C_{20}. The simulated annealing method located two different dense lamellar structures for the solid phase: a monoclinic structure with the chain axes normal to the layer plane and a triclinic structure with the chain axes tilted away from the normal to the layer plane, as illustrated in Figure 3. The close packed densities are very similar for the two structures. The data on the free energy for these structures is given in Table 4.

We first consider the C_{18} system. The pressure−density equations of state and phase transition are shown in Figure 10.

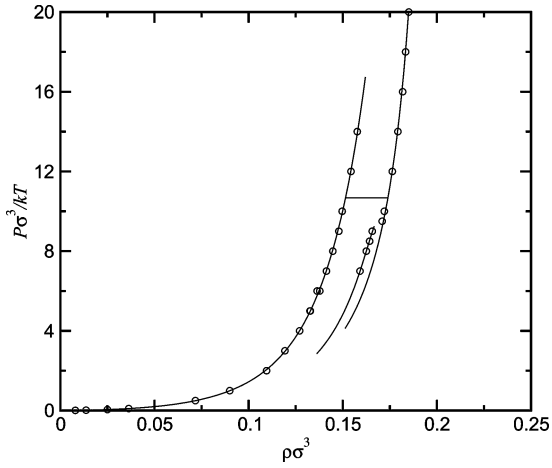

Figure 8. Pressure−density equation of state of the C_{13} system. The points are our Monte Carlo simulation resultsm and the lines give the fits from eqs 12 and 13. The phase transitions are indicated by horizontal lines. The uncertainty in the density is much smaller than the symbol size used in the figure.

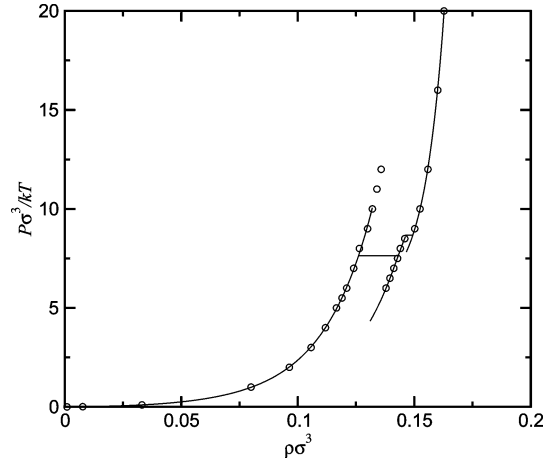

Figure 9. Pressure−density equation of state of the C_{15} system. The points are our Monte Carlo simulation results, and the lines give the fits from eqs 12 and 13. The phase transitions are indicated by horizontal lines. The uncertainty in the density is much smaller than the symbol size used in the figure.

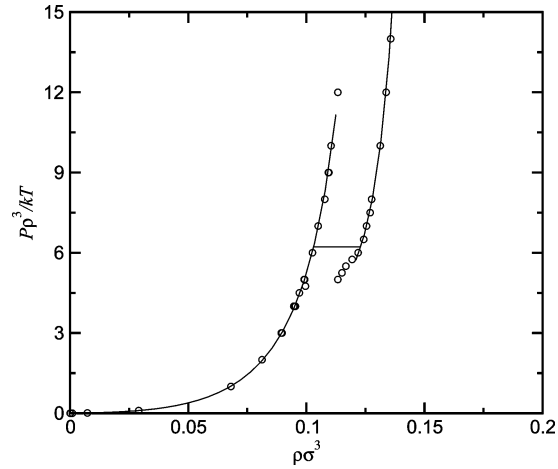

Figure 10. Pressure−density equation of state of the C_{18} system. The points are our Monte Carlo simulation results, and the lines give the fits from eqs 12 and 13. The phase transitions are indicated by horizontal lines. The uncertainty in the density is much smaller than the symbol size used in the figure.

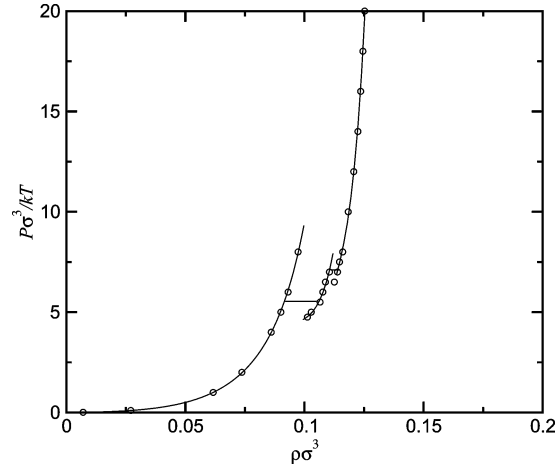

Figure 11. Pressure−density equation of state of the C_{20} system. The points are our Monte Carlo simulation results, and the lines give the fits from eqs 12 and 13. The phase transitions are indicated by horizontal lines. The uncertainty in the density is much smaller than the symbol size used in the figure.

The calculations indicate that for our C_{18} model, only the fluid phase and triclinic solid are stable with no stable rotator phase in the system. Although the monoclinic phases are not stable for this chain length of our model, it is interesting to note that the monoclinic rotator phase has a domain of stability with respect to the crystalline monoclinic phase. This contrasts with the triclinic solid, in which the rotator phase has no domain of stability. Evidently, having the chains aligned normal to the plane of the lamellae facilitates the stability of the monoclinic rotator phase.

Figure 11 shows the pressure−density equation of state and phase transitions calculated for the C_{20} model. We have found that the monoclinic solid is slightly more stable than the triclinic solid. This facilitates the stability of a rotator phase, and we see that this phase has a domain of stability. This result is not fully consistent with experiment, which indicates that the triclinic structure is the stable one for C_{20}.[33] However, the rotator phase can be observed as a metastable phase on freezing the liquid but not on the heating the crystalline solid.[18,19] Experiments also show that the monoclinic structure becomes stable above a chain length of C_{26}, and the rotator phase is stable for those systems.[33,37,38] Although our simulation results do not show exactly the same phase behavior for C_{20}, they show a similar tendency of the phase behavior versus chain length. Our simulations show evidence that the stable solid structure changes from a triclinic structure for shorter chains to a monoclinic structure for longer chains, and onset of stability of the monoclinic crystal coincides with that of the rotator phase.

IV. Summary and Conclusions

In this paper, we have extended earlier work on using hard sphere chain models to solid−fluid phase equilibrium for *n*-alkanes[1] to longer chain systems where rotator phases appear. An athermal torsional potential that admitted the possibility of gauche conformations was used. Extensive calculations of the thermodynamic properties for the fluids and solids were carried out using Monte Carlo simulations. The crystal structures used were based on close packed structures determined by simulated annealing. The initial states for the annealing calculation were based on experimental crystal structures for *n*-alkanes. For even carbon numbers, we found triclinic and monoclinic structures, both of which have been seen in experiments. For odd carbon numbers, we found a triclinic structure that differs from the

experimentally determined orthorhombic structure most significantly because of the existence of only one orientation around the chain axis within each layer, rather than two. We determined the pressure density equations of state, the free energy, and orientational order parameters that indicate the formation of a rotator phase.

For odd carbon numbers, the triclinic structure (the experimental structure for short chains with odd carbon numbers) was found to be stable for all chain lengths considered. The rotator phase was observed during the simulations for all odd-carbon-number *n*-alkanes studied. However, we find that it is thermodynamically stable only for C_{15} chains and beyond. For even carbon numbers, we studied C_{18} and C_{20} in detail. The triclinic structure is stable for C_{18}, but no stable rotator phase appears. The monoclinic structure is stable for C_{20}, and this system has a stable rotator phase between the ordered crystalline and fluid phases.

Although our results do not precisely track the experimental observations for *n*-alkane systems, important qualitative trends are reproduced correctly. First of all, both the simulations and experiment show that the stable solid state of even-carbon-number *n*-alkanes varies from triclinic to monoclinic structure with an increase in the chain length. Our simulations also share the feature with experimental results that the rotator phase more easily forms for phases in which the chain axes are perpendicular to the planes of the lamellae in the solid. That is the reason why the rotator phase is observed experimentally for odd-carbon-number *n*-alkanes above C_9 but is not seen in the even-carbon-number *n*-alkanes until the chain length reaches C_{20}. A more sophisticated model, most likely one with explicit treatment of the hydrogen atoms, would perhaps give a more precise correspondence to experiment, but it is nevertheless pleasing that the united atom hard sphere chain model displays so much of the physics of these systems.

References and Notes

(1) Malanoski, A. P.; Monson, P. A. *J. Chem. Phys.* **1999**, *110*, 664. *J. Chem. Phys.* **2003**, *118*, 995.
(2) Boese, R.; Weiss, H.-C.; Blaser, D. *Angew. Chem., Int. Ed.* **1999**, *38* (7), 988.
(3) Müller, A. *Proc. R. Soc. London* **1928**, *120*, 455.
(4) Müller, A. *Proc. R. Soc. London, Ser. A* **1932**, *138*, 514.
(5) Smith, A. E. *J. Chem. Phys.* **1953**, *21*, 229.
(6) Carievich, A.; Doucet, J.; Denicolo, I. *Phys. Rev. B* **1985**, *32*, 4164.
(7) Turnbull, D.; Cormia, R. L. *J. Chem. Phys.* **1961**, *34*, 820.
(8) Broadhurst, M. G. *J. Res. Natl. Bur. Stand. A* **1962**, *66A*, 241.
(9) Doucet, J.; Denicolo, I.; Craievich, A. *J. Chem. Phys.* **1981**, *75* (3), 1523.
(10) Doucet, J.; Denicolo, I.; Craievich, A.; Collet, A. *J. Chem. Phys.* **1981**, *75* (10), 5125.
(11) Doucet, J.; Denicolo, I.; Craievich, A.; Germain, C. *J. Chem. Phys.* **1984**, *80*, 1647.
(12) Denicolo, I.; Doucet, J.; Craievich, A. F. *J. Chem. Phys.* **1983**, *78* (3), 1465.
(13) Guillaume, J.; Doucet, J.; Sourisseau, C.; Dianoux, A. J. *J. Chem. Phys.* **1989**, *91*, 2555.
(14) Sirota, E. B.; King, H. E.; Singer, D. M., Jr.; Shao, H. H. *J. Chem, Phys.* **1993**, *98*, 5809.
(15) Sirota, E. B.; Singer, D. M. *J. Chem. Phys.* **1994**, *101*, 10873.
(16) Kitamaru, R.; Horii, F.; Nakagawa, M.; Takamizawa, K.; Urabe, Y.; Ogawa, Y. *J. Mol. Struct.* **1995**, *355*, 95.
(17) Sirota, E. B.; Herhold, A. B. *Polymer* **2000**, *41*, 8781.
(18) Seyer, W. F.; Patterson, R. F.; Keays, J. L. *J. Am. Chem. Soc.* **1944**, *66* (2), 179.
(19) Sirota, E. B.; King, H. E.; Hughes, G. J., Jr.; Wan, W. K. *Phys. Rev. Lett.* **1992**, *68*, 492.
(20) Whittington, S. G.; Chapman, D. *Trans. Faraday Soc.* **1965**, *61*, 2656.
(21) Mazo, M. A.; Oleynik, E. F.; Balabaev, N. K.; Lunevskaya, L. V.; Grivtsov, A. G. *Polym. Bull.* **1984**, *12*, 303.
(22) Ryckaert, J.-P.; McDonard, I. R.; Klein, M. L. *Mol. Phys.* **1989**, *67*, 957.
(23) Ryckaert, J.-P.; Klein, M. L.; McDonard, I. R. *Mol. Phys.* **1994**, *83*, 439.
(24) Ryckaert, J.-P.; Klein, M. L.; McDonard, I. R. *Phys. Rev. Lett.* **1987**, *58*, 689.
(25) Martonak, R.; Paul, W.; Binder, K. *J. Chem. Phys.* **1997**, *106*, 8918.
(26) Fujiwara, S.; Sato, T. *J. Chem. Phys.* **1999**, *110*, 9757.
(27) Mavrantza, I.-E.; Prentzas, D.; Mavrantza, V. G.; Galiotis, C. *J. Chem. Phys.* **2001**, *115*, 3937.
(28) Shen, W.-N.; Monson, P. A. *J. Chem. Phys.* **1995**, *103*, 9756.
(29) Malanoski, A. P.; Monson, P. A. *J. Chem. Phys.* **2000**, *112*, 2870.
(30) Cao, M.; Monson, P. A. *J. Chem. Phys.* **2004**, *120*, 2980.
(31) Ryckaert, J.-P.; Bellemans, A. *Discuss. Faraday Soc.* **1978**, *110*, 95.
(32) Padilla, P.; Toxvaerd, S. *J. Chem. Phys.* **1991**, *94*, 5650.
(33) Kitaigorodsky, A. I. *Molecular Crystals and Molecules*; Academic: New York, 1973.
(34) Frenkel, D.; Ladd, A. J. C. *J. Chem. Phys.* **1984**, *81*, 3188.
(35) Polson, J. M.; Trizac, E.; Pronk, S.; Frenkel, D. *J. Chem. Phys.* **2000**, *112*, 5339.
(36) Siepmann, J. I.; Frenkel, D. *Mol. Phys.* **1992**, *75*, 59.
(37) Turner, W. R. *Ind. Eng. Chem. Prod. Res. Dev.* **1997**, *10* (3), 238.
(38) Ohlberg, S. M. *J. Chem. Phys.* **1959**, *63*, 248.
(39) Parrinello, M.; Rahman, A. *Phys. Rev. Lett.* **1980**, *45*, 1196.

JP902887W